Available online at www.sciencedirect.com
SCIENCE DIRECT®
Journal of Sound and Vibration 267 (2003) 851–865
JOURNAL OF SOUND AND VIBRATION
www.elsevier.com/locate/jsvi

Active vibration control for structural–acoustic coupling system of a 3-D vehicle cabin model

Chul Ki Song[a,*], Jin Kwon Hwang[b], Jang Moo Lee[c], J. Karl Hedrick[d]

[a] School of Mechanical Engineering, ReCAPT, Gyeongsang National University, Gyeongnam, South Korea
[b] Department of Electrical Engineering, Woosuk University, Jeonbuk, South Korea
[c] School of Mechanical and Aerospace Engineering, Seoul National University, Seoul, South Korea
[d] Department of Mechanical Engineering, UC Berkeley, Berkeley CA, USA

Received 19 September 2000; accepted 18 October 2002

Abstract

This paper presents an active vibration control system for use with structural–acoustic coupling system using piezoelectric actuators and piezoelectric sensors. For modelling a complicated 3-D vehicle cabin model, the structural–acoustic coupling system is analyzed by combining the structural data from modal testing with the acoustic data from the finite element method. Through the structural–acoustic analysis program, the control plate and the control modes are selected, which are most effective for attenuating its noise. A robust LQG controller with two sensor signal filters is designed to remove the experimental problems such as the spillover effect due to uncontrolled modes. The robust LQG controller for the structural–acoustic coupling system can reduce the interior noise of the cavity as well as the structural vibration of the cabin.

1. Introduction

Vibration and interior noise in vehicles have recently become more important as passengers demand a more comfortable ride. They are mainly caused from power train and road input, and are also caused from vibrating structures, which are actuated by rotating the power train and driving the vehicle on the road. Among the various vehicle noise problems, structural-borne noise such as booming, which is due to the coupling between the structural vibration and the interior noise, has been investigated [1–4]. Acoustic mode shapes and acoustic natural frequencies are dependent upon the design of a vehicle cavity, so it may be not easy to modify them in order to reduce the structural-borne noise. Low-frequency noise in the passenger vehicle (in approximately

*Corresponding author. Tel.: +55-751-6074.
E-mail address: cksong@nongae.gsnu.ac.kr (C.K. Song).

0022-460X/03/$ - see front matter © 2002 Elsevier Science Ltd. All rights reserved.
doi:10.1016/S0022-460X(02)01553-5

the 20–200 Hz frequency range) is of primary interest, and particularly that noise which is generated by the structural vibration of the wall panel of the vehicle cabin [2].

Piezoelectric materials such as lead zirconate titanate (PZT) and poly vinylidene fluoride (PVDF) have been used as sensors and actuators in vibration control of flexible structures. The piezoelectric materials are accurate in sensing and actuation, small, low weight, low cost, and generate large forces without reaction. Many researchers have applied piezoelectric materials to attenuate acoustic noise. Dimitriadis and Fuller [5] theoretically have investigated the active control of sound transmission though a plate using piezoelectric materials, Fuller et al. [6,7], and Clark and Fuller [8] experimentally have studied the active control of sound radiation from a panel using piezoelectric materials. Sonti and Jones [9] have studied the control of sound radiation from a shell structure. Jones and Fuller [10], and Fuller and Hansen [11] have shown attenuation of interior noise by active vibration control on cylinder and aircraft using piezoelectric materials. Snyder and Hansen [12] have derived the optimal control equation of the structural–acoustic coupling system. Griffin et al. [13] have studied the feedback control of structurally radiated sound into enclosed structures.

In this study, the structural vibration control instead of the fully structural–acoustic coupling control is used for reducing not only the structural vibration but also the interior noise though the structural–acoustic coupling analysis and the LQG structural vibration control. The active vibration control for the structural–acoustic coupling system using piezoelectric materials is presented. In order to solve the difficulty in modelling a complicated 3-D vehicle cabin, the structural–acoustic coupling system is analyzed by combining the structural data which are obtained by modal testing [14] with the acoustic data which are obtained by the finite element method (FEM). Through the contribution analysis of the coupled system by acoustic–structural analysis program (ASTAP) [4], a controlled plate and controlled modes are selected, which are most effective for attenuating its noise. Piezoelectric actuators and piezoelectric sensors for control are co-located in order to reduce the spillover effect. The design of controllers is on the basis of a multi-input multi-output (MIMO) system [15,16]. The modal parameters of the structure including the piezoelectric actuators and sensors can be obtained by the identification method [17] with band-pass filters. And to solve the experimental problems such as the spillover effect due to uncontrolled modes, a robust LQG controller is designed, using two sensor signal filters. One is a low-pass filter for attenuating uncontrolled modal signals, and the other is a high-pass filter for reducing DC bias in the sensor signal and making the gain of the robust controller higher. These high- and low-pass filters can also attenuate temporal noise. The robust LQG controller for structural vibration control can reduce the interior noise of the cavity as well as the structural vibration of the cabin.

2. Interior sound pressure of a 3-D cavity

Interior sound pressure at any position r of a 3-D cavity is represented by c_{as} or the acoustic–structural modal coupling coefficient c'_s as follows [4]:

$$p(r) = \rho c^2 \sum_{a=1}^{na} \sum_{s=1}^{ns} \varphi_a(r) z_a c_{as} z_s \{\phi_s\}^{\mathrm{T}} \{F\}, \tag{1}$$

$$z_a \triangleq \frac{-j\omega}{\Omega_a^2 - \omega^2 + j\xi_a\omega}, \quad z_s \triangleq \frac{j\omega}{\Omega_s^2 - \omega^2 + j\xi_s\Omega_s^2},$$

$$c_{as} \triangleq \int_\Gamma \varphi_a(r_\Gamma)\phi_s(r_\Gamma)\,d\Gamma, \quad c'_{as} \cong \frac{c_{as}}{\Omega_s^2 - \Omega_a^2} \quad \text{(for small damping)},$$

where subscript a and s mean the ath acoustic mode and the sth structural mode, na and ns are the acoustic modal number and structural modal number, φ_a and ϕ_s are the acoustic mode shape and the structural mode shape, respectively. ξ_a and ξ_s are the acoustic modal damping coefficient and the structural modal damping coefficient, ρ and c are the mass density of air and the speed of sound in air, and Ω and z are the resonance frequency and the impedance, respectively. Γ means the boundary between the structure of a 3-D cabin and the acoustics of a cavity, and F means the applied force on the structural system. Especially, c'_{as} is the approaching coefficient between the acoustic resonance frequency and the structural resonance frequency, which is determined by the characteristics of the acoustic–structural system, not by the external force conditions or the internal measurement points.

3. Structural–acoustic coupling system of a 3-D vehicle model

3.1. Structural modes of the 3-D vehicle cabin

Fig. 1 is a half-scaled model of a passenger vehicle, which is hanged to flexible rubber strings in order to reduce the stiffness effect by boundary condition.

In a 3-D complicated structure like a vehicle cabin, it is not easy by the FEM to accurately obtain the broadbanded structural mode shapes and those corresponding damping coefficients. The structural data are obtained by modal testing instead of the FEM. An impact hammer, low-mass accelerometers, a HP Front End, and a HP715/75 Workstation are used for accurately measuring the structural mobility of the boundary. The multi-peak fitting method [18] is used for the curve fitting procedure using a total of 326 frequency response functions obtained from 225 actuating and measuring positions. Even though low-frequency noise in the real passenger vehicle

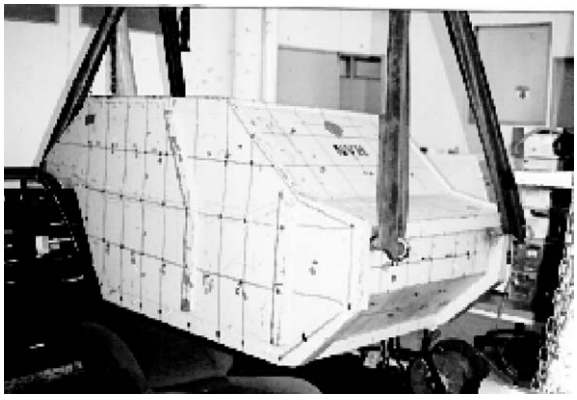

Fig. 1. Half-scaled model of a passenger vehicle.

(in approximately the 20–200 Hz frequency range) is of primary interest [2,4], 30–300 Hz frequency range is mainly of interest in this half-scaled model of a passenger vehicle.

More than 50 resonance peaks exist in the frequency range of 30–300 Hz and its corresponding damping ratios are mostly small, less than 0.1%. The significant modes selected in 50 measured structural modes are S1 (74.3 Hz), S2 (120.9 Hz), S3 (162.2 Hz), S4 (243.9 Hz), and S5 (272.3 Hz), which contribute to the interior noise of the 3-D cavity. Fig. 2 shows structural mode shapes which are obtained by modal testing.

3.2. Acoustic modes of the 3-D vehicle cavity

Fig. 3 shows the acoustic finite element model of a 3-D vehicle cavity, whose boundaries are assumed as solid walls. Air density is 1.21 kg/m^3, and air velocity is assumed as 340 m/s. 1293 nodes and 5990 elements are used. For the comparison, acoustic modes and frequencies are experimentally determined through a resonance test. It is not easy to determine acoustic modal data experimentally because 3-D acoustic modal testing should be done in the cabin. The acoustic natural frequencies by the FEM are near to those from experiments, as can be seen in Table 1. The

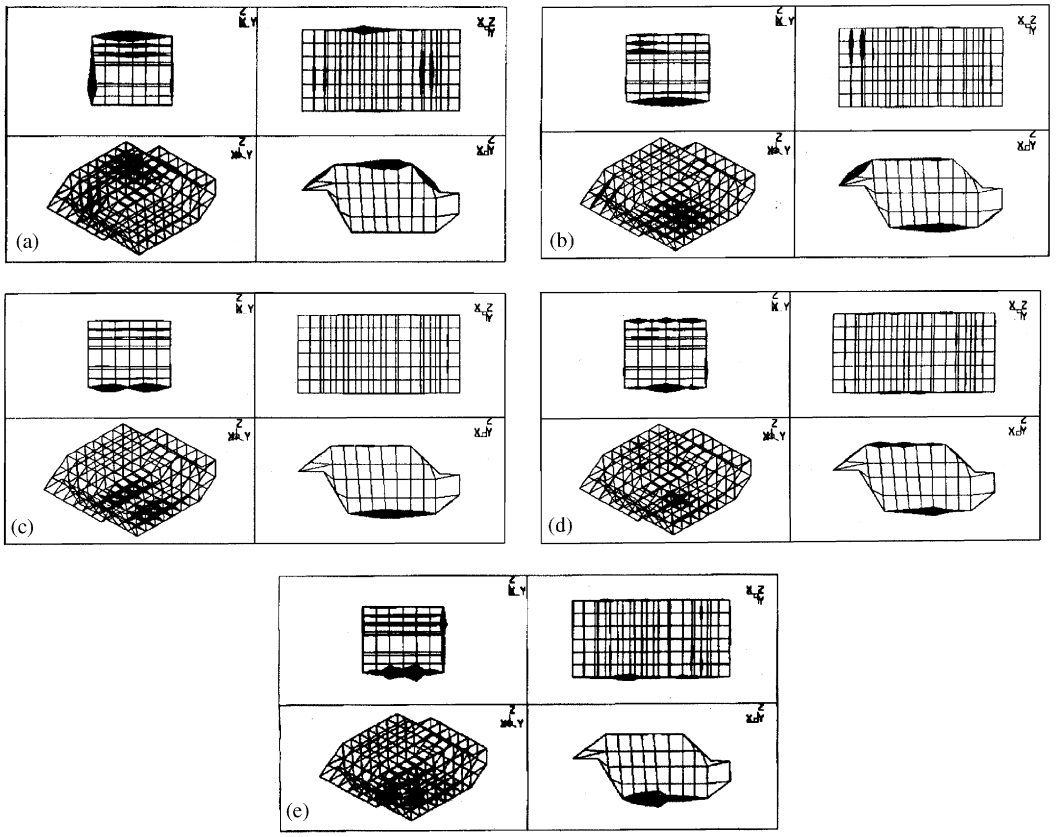

Fig. 2. Structural mode shapes of a 3-D vehicle cabin model, which are obtained by modal testing: (a) 74.3 Hz, (b) 120.9 Hz, (c) 162.2 Hz, (d) 243.9 Hz, and (e) 272.3 Hz.

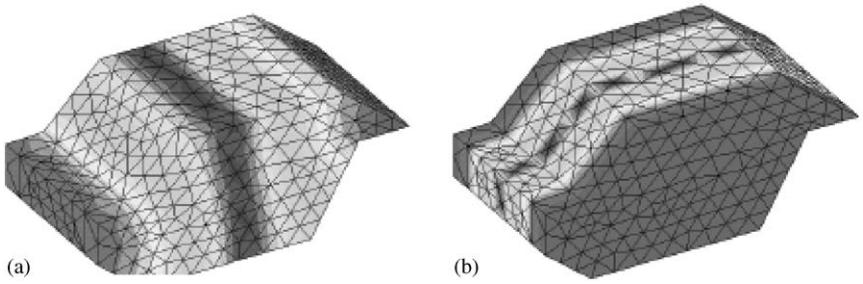

Fig. 3. Acoustic mode shapes by the FEM: (a) A1 mode (175 Hz), and (b) A2 mode (262 Hz).

Table 1
Acoustic natural frequencies of a 3-D vehicle cavity model

Acoustic mode	Mode shape	Natural frequency (Hz)	
		Experiment	Finite element method
A1	(1, 0, 0)	177	175
A2	(0, 1, 0)	257	262

reason why the measured and calculated resonance frequencies do not match exactly may be due to a change from the rigid-walled natural frequencies. Another reason may be due to the shape difference between the real model and the finite element model of a 3-D vehicle cavity.

3.3. Structural–acoustic coupling system of the 3-D vehicle model

Fig. 4 shows the structural–acoustic frequency response functions by experiment, which are actuated at the center of the front left floor to actuate symmetric modes and antisymmetric modes simultaneously, and are measured at the driver's hearing point and the right rear hearing point. Main peaks of interior noise appear at the resonance frequencies of the cabin's structural modes which act globally including the floor panel, while any peaks of interior noise are not seen at the resonance frequencies of the cabin's structural modes which act locally. Using the fact that local structure modes have little effect on the interior noise, and that the magnitude of sound pressure level varies greatly at a certain frequency according to the measuring position, it can be inferred experimentally that the structural mode and the acoustic mode are coupled with each other. For example, the sound pressure level near to the frequency of the first acoustic mode A1 varies greatly according to measuring positions in the cavity, which means the structural–acoustic modal coupling coefficient is high due to close resonance frequencies between S3 and A1, and because the driver's hearing point is near the nodal plane of the first acoustic mode, the peak A1 cannot be seen in Fig. 4(a). The sound pressure level at frequencies nears the resonance frequencies of the structural mode S2 varies little according to the measuring positions in the cavity, which means that the structural–acoustic coupling sensitivity between S2 and A1 is relatively low.

Fig. 5 shows the structural–acoustic frequency response functions by using the coupling analysis program ASTAP [4], which are actuated and measured at the same positions as Fig. 4.

Comparing the numerical results in Fig. 5 with the experimental results in Fig. 4, overall characteristics are similar to each other. The structural–acoustic coupling system can be verified, which is obtained by combining the structural data from modal testing with the acoustic data from the FEM. Some differences between the numerical results and the experimental results may be caused from the difference of measuring points between experiments and analyses, the asymmetric structure of the cabin model for experiments, the inexact acoustic resonance frequency between experiments and analyses, the uncertainty of damping coefficients and phases in structural modes, existing acoustic damping characteristics. And the differences may also be due to neglecting the stiffness residues.

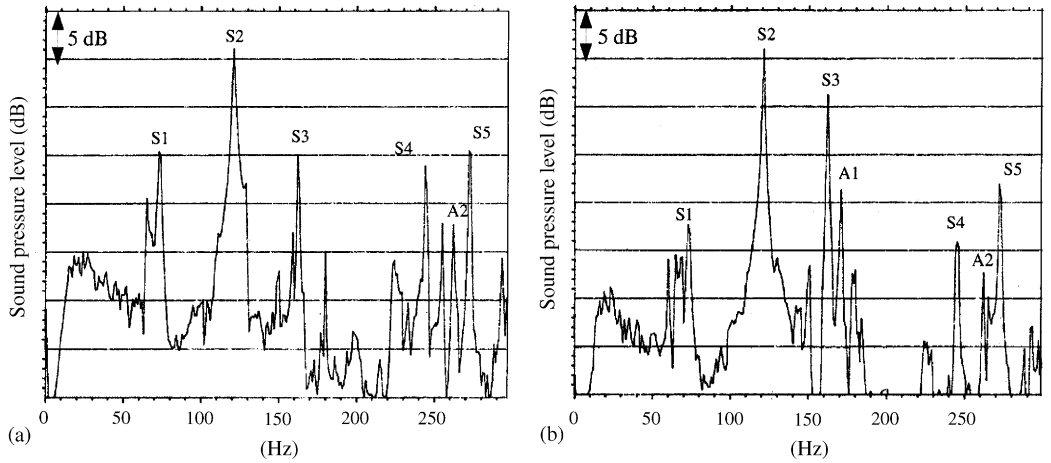

Fig. 4. Structural–acoustic frequency response functions by experiments: (a) driver's hearing point and (b) rear right hearing point.

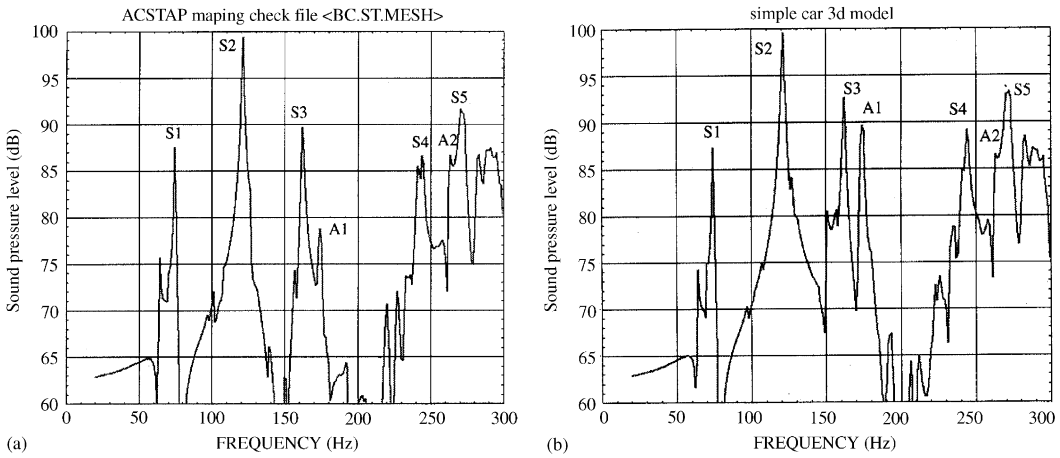

Fig. 5. Structural–acoustic frequency response functions by ASTAP: (a) driver's hearing point and (b) rear right hearing point.

Table 2 shows the dominant structural–acoustic modal coupling coefficients. Coefficients c'_{11}, c'_{23}, c'_{24}, and c'_{25} are relatively large, which means that the structural modes of S1, S3, S4, and S5 can generate high levels of noise, when they are excited. The structural mode S1 is strongly coupled with the first acoustic mode A1, and the structural modes of S3, S4, and S5 are strongly coupled with the second acoustic mode A2. The level, of course, is also influenced by the exciting and measuring positions, which are too complex to consider in detail for real ears.

Fig. 6 shows the boundary panel contribution [4] to the dominant structural–acoustic modal coupling coefficients, which means that the darker the area is, the bigger the contribution to the coupling coefficient is. Fig. 6(a) shows that the front window panel has the largest contribution to the coupling coefficient c'_{11}, and Figs. 6(b)–(d) show that the floor plate has the largest coupling

Table 2
Structural–acoustic modal coupling coefficients ($c'_{as} \times 10^4$)

Structural modes		Acoustic modes	
		A1 175 Hz	A2 262 Hz
S1	74.3 Hz	−4.5	1.1
S2	120.9 Hz	−1.5	0.0
S3	162.2 Hz	−2.6	−6.0
S4	243.9 Hz	−0.6	−6.7
S5	272.3 Hz	−0.1	6.7

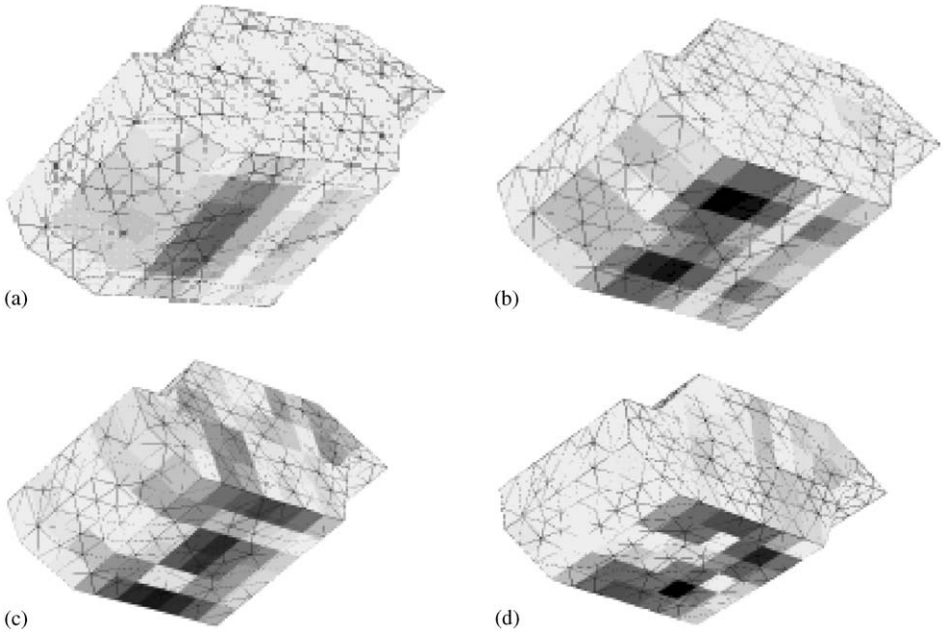

Fig. 6. Boundary panel contribution to the dominant structural–acoustic modal coupling coefficients (inclined bottom view): (a) contribution to c'_{11}, (b) contribution to c'_{23}, (c) contribution to c'_{24}, and (d) contribution to c'_{25}.

coefficients of c'_{23}, c'_{24}, and c'_{25}. Therefore, when the floor panel is selected as a control panel for attenuating structural vibration, the interior noise of the cavity can also be attenuated effectively. This control panel directly receives the power train vibration transferred through engine mounts as well as the road vibration transferred through suspensions.

4. Structural–acoustic coupling system

4.1. Determination of control modes in a 3-D vehicle model

A half-sized 3-D vehicle model is used for structural–acoustic coupling system, as shown in Fig. 7. The floor panel to be controlled is reinforced by two longitudinal beams and a lateral beam, like that of the actual vehicle. The mode shapes of the structure are very complicated and its modal density is much larger than the acoustic modal density. The more complicated the mode shapes of the structure are, the more difficult it is to select actuating positions and measuring positions. And the higher the modal density is, the more problems that occur in control experiments. Many modes within broad frequency band cannot be simultaneously controlled in real time, due to limited processing time. From these reasons, only a few modes must be controlled in a structure with high modal density. And the spillover effect will occur at the uncontrolled modes with resonance frequencies near to the resonance frequencies of the controlled modes. To reduce the spillover effect, low- and high-pass filters can be used to filter uncontrolled modal signals.

Three structural modes, which effect significantly on the interior noise of the vehicle cavity, are selected as control modes in the control panel. They are S3 (162.2 Hz), S4 (243.9 Hz), and S5 (272.3 Hz). Two co-located piezoelectric actuators and sensors are attached at positions where these control modes can be measured and actuated very well. The first actuator and sensor are relatively good for actuating and measuring modes S3 and S4 and the second actuator and sensor are relatively good for actuating and measuring modes S3 and S5. These two pairs of actuators and sensors also actuate and measure a weakly excited uncontrolled mode whose resonant

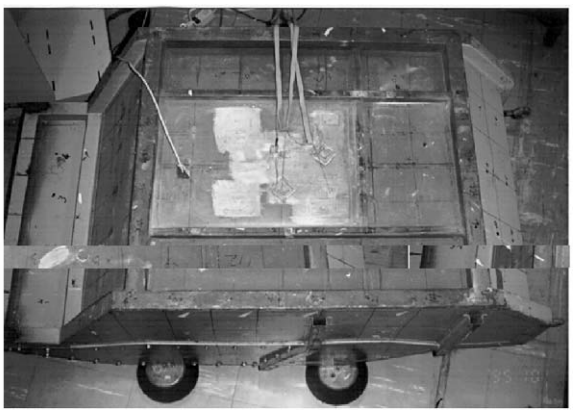

Fig. 7. Vehicle cabin model with bonded piezoelectric materials for a structural vibration control (bottom view).

frequency is 304.1 Hz. The piezoelectric material in the experiment is G1195 PZT [19]. The density is 7600 kg/m^3, the strain constant is 166×10^{-12} m/V, the permittivity is 151×10^{-10}, Young's modulus is 63×10^9 N/m^2, and the Poisson ratio is 0.31.

4.2. Design of a robust LQG controller

The model in the state space for the three control modes, S3, S4, and S5, can be obtained as

$$\dot{w}(t) = Aw(t) + Bu(t),$$
$$z(t) = Cw(t), \tag{2}$$

where the state vector is $w(t) = [w_1(t), \dot{w}_1(t), w_2(t), \dot{w}_2(t), w_3(t), \dot{w}_3(t)]^{\mathrm{T}}$, the actuator input vector is $u(t) = [u_1(t), u_2(t)]^{\mathrm{T}}$, the sensor output vector is $z(t) = [z_1(t), z_2(t)]^{\mathrm{T}}$. The matrices A, B, and C are the system matrices, which can be obtained from experimental data using digital spatial filters [17]

$$A = \mathrm{diag}(A_1, A_2, A_3),$$

$$A_1 = \begin{bmatrix} 0 & 1 \\ -1038100 & -2.6491 \end{bmatrix}, \quad A_2 = \begin{bmatrix} 0 & 1 \\ -2349200 & -3.4449 \end{bmatrix}, \quad A_3 = \begin{bmatrix} 0 & 1 \\ -2927900 & -2.0635 \end{bmatrix},$$

$$B = \begin{bmatrix} 0 & -223.5 & 0 & 723.2 & 0 & -2341.4 \\ 0 & 60.4 & 0 & -1985.5 & 0 & -483.0 \end{bmatrix}^{\mathrm{T}},$$

$$C = \begin{bmatrix} 1 & 0 & -0.3208 & 0 & 1 & 0 \\ 0.2554 & 0 & 1 & 0 & 0.2345 & 0 \end{bmatrix}.$$

Fig. 8 is the block diagram of experiments for a structural vibration control. The LQG controller is digitally implemented with a TMS320C30 DSP chip set and A/D and D/A converters. The A/D and D/A converters have a 12-bit resolution and maximum absolute voltage for these converters is 5 V. Low-pass filters with bandwidth of 310 Hz are used in sensor signals to

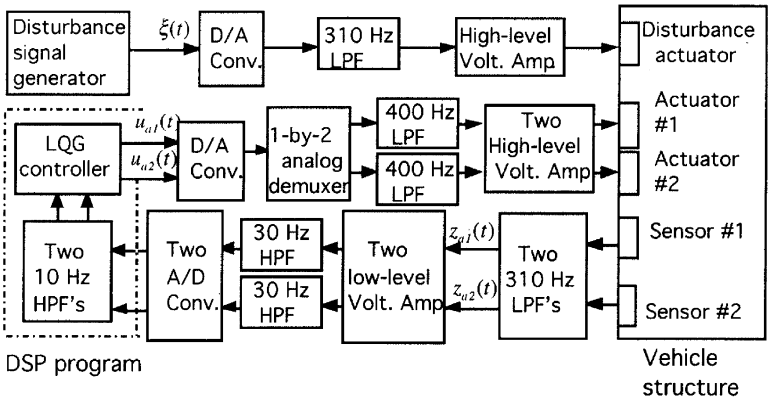

Fig. 8. Block diagram for a structural vibration control.

attenuate not only high-frequency noise but also uncontrolled modes with resonance frequencies more than 310 Hz.

There is a small DC bias in the data sampled with the A/D converters. This is due to voltage deviation of the A/D converter, as well as the ground voltage difference between electrical circuit boards and the plate with piezoelectric sensors. The DC bias drives the LQG controller, which has a high gain at 0 Hz, to the saturation limit of the D/A converters. Therefore, 10 Hz second order digital high-pass filters are introduced for the sampled data. For good reduction of vibration, the LQG controller may have a high gain. But the higher the LQG controller gain is, the more unstable the whole control system may be. The unstable modes appear in the lower frequency range than the control frequencies. Therefore, 30 Hz high-pass filters are additionally used for solving the problem in the low-frequency range, and the high gain of the LQG controller can be obtained. The step-wave signal per each sampling time in the D/A converter also makes high-frequency noise. This noise also becomes another disturbance in the structural–acoustic coupling model of the vehicle cabin as well as the radiation sound source. To prevent this effect, 400 Hz low-pass analog filters are added after the D/A converter.

The cutoff frequency, 30 Hz, of the high-pass filters is significantly smaller than the lowest modal frequencies to be controlled, and its dynamics can be neglected in designing the controller. But because the frequency, 310 Hz, of the low-pass filters in the sensor signal is close to the highest frequency to be controlled, the filtering affects the phases and magnitudes of the modes to be controlled. Therefore, it is necessary to use an augmented system, which includes the dynamics of the low-pass filters in designing the LQG controller. It is desirable that the augmented system becomes minimum phase. The dynamics of the Butterworth filter can be expressed as

$$\begin{aligned} \dot{v}_i(t) &= Kv_i(t) + Lz_i(t), \\ & \qquad\qquad i = 1, 2, \\ r_i(t) &= Mv_i(t), \end{aligned} \tag{3}$$

$$K = \begin{bmatrix} -2.7542 \times 10^3 & -3.7939 \times 10^6 \\ 1 & 0 \end{bmatrix}, \quad L = \begin{bmatrix} 1 \\ 0 \end{bmatrix}, \quad M = \begin{bmatrix} 0 & 6.0163 \times 10^6 \end{bmatrix},$$

where $v_i(t)$ is the 2×1 state vector of the filter for the ith sensor, $r_i(t)$ is the scalar output of the filter for the ith sensor, and K, L, M are the system matrices of the filters.

Including the process noise and the measurement noise, the dynamics for the augmented system can be expressed as

$$\begin{aligned} \dot{w}_a(t) &= A_a w_a(t) + B_a u_a(t) + \xi(t), \\ z_a(t) &= C_a w_a(t) + \theta(t), \end{aligned} \tag{4}$$

where $w_a(t) = [w^{\mathrm{T}}(t), v_1^{\mathrm{T}}(t), v_2^{\mathrm{T}}(t)]^{\mathrm{T}}$, $u_a(t) = u(t)$, and $z_a(t) = [r_1(t), r_2(t)]^{\mathrm{T}}$. The matrices A_a, B_a, C_a are the augmented system matrices, $\xi(t)$ is a process noise vector, and $\theta(t)$ is a measurement noise vector. To design the LQG controller for the augmented system, the covariance matrices of $\xi(t)$ and $\theta(t)$ must be found. Since $\xi(t)$ is not measurable, the covariance matrix Ξ of $\xi(t)$ is set as follows:

$$\Xi = \alpha B_a B_a^{\mathrm{T}}. \tag{5}$$

Here, the noise to the low-pass filters is assumed to be zero, and the power of $\xi(t)$ is adjusted by α. Since the gain of the LQG controller is proportional to $\sqrt{\alpha}$, α can be used as a design parameter to make the controller robust for the uncontrolled modes. Making α smaller, the controller becomes more robust, while the vibration is less attenuated.

The covariance matrix Θ of $\theta(t)$ can be computed from the resolution of the measurement device, i.e., from the voltage resolution of A/D converters for sampled sensor signals. With the assumption that the density function of $\theta(t)$ is uniformly distributed, the covariance matrix Θ becomes

$$\Theta = \frac{V^2}{12 \times 2^b} I_m, \tag{6}$$

where V is the voltage range of the A/D converter and b is the number of bits for the A/D converter.

For the design of the LQG controller, the cost function is

$$J = \lim_{T \to \infty} E\left[\frac{1}{T}\int_0^T \left\{w_a^{\mathrm{T}}(t) Q w_a(t) + u_a^{\mathrm{T}}(t) u_a(t)\right\} \mathrm{d}t\right], \tag{7}$$

where $E[\cdot]$ is the expected value and Q is the weighting matrix for the states. The weighting matrix Q is chosen so that the lower frequency modes are weighted more, and the states of the modal displacements are weighted more than the states of the modal velocities

$$Q = \mathrm{diag}(\,2000 \quad 200 \quad 800 \quad 80 \quad 300 \quad 30 \quad 10 \quad 10 \quad 10 \quad 10\,).$$

For experiments, vibration of the cabin is generated with the disturbance generator, which is driven by band-pass pseudo-random noise of 100–310 Hz. Good performance and stability are shown in the simulation considering all design parameters. However, in the actual experiments, an unexpected problem occurs, which is an unstable effect at 505 Hz. The mode cannot be measured well and cannot be actuated well before controlling. This effect may occur from the control system dynamics, which is changed by neglecting the characteristics of the analog filters and by high gain in designing the controller. To remove the unstable effect, the mode of 505 Hz is also added to the model in this study. The revised system matrix and the revised weight matrix including the four modes are as

$$A = \mathrm{diag}(A_1, A_2, A_3, A_4), \quad A_4 = \begin{bmatrix} 0 & 1 \\ -10068000 & -2.1141 \end{bmatrix},$$

$$B = \begin{bmatrix} 0 & -223.5 & 0 & 723.2 & 0 & -2341.4 & 0 & -8859.3 \\ 0 & 60.4 & 0 & -1985.5 & 0 & -483.0 & 0 & -17050.0 \end{bmatrix}^{\mathrm{T}},$$

$$C = \begin{bmatrix} 1 & 0 & -0.3208 & 0 & 1 & 0 & 0.7239 & 0 \\ -0.2554 & 0 & 1 & 0 & 0.2345 & 0 & 1 & 0 \end{bmatrix}.$$

4.3. Experimental results

Figs. 9 and 10 are the experimental results at sensors 1 and 2, respectively. Figs. 9(a), (b), 10(a) and (b) show the uncontrolled time response and the controlled time response, and Figs. 9(c) and

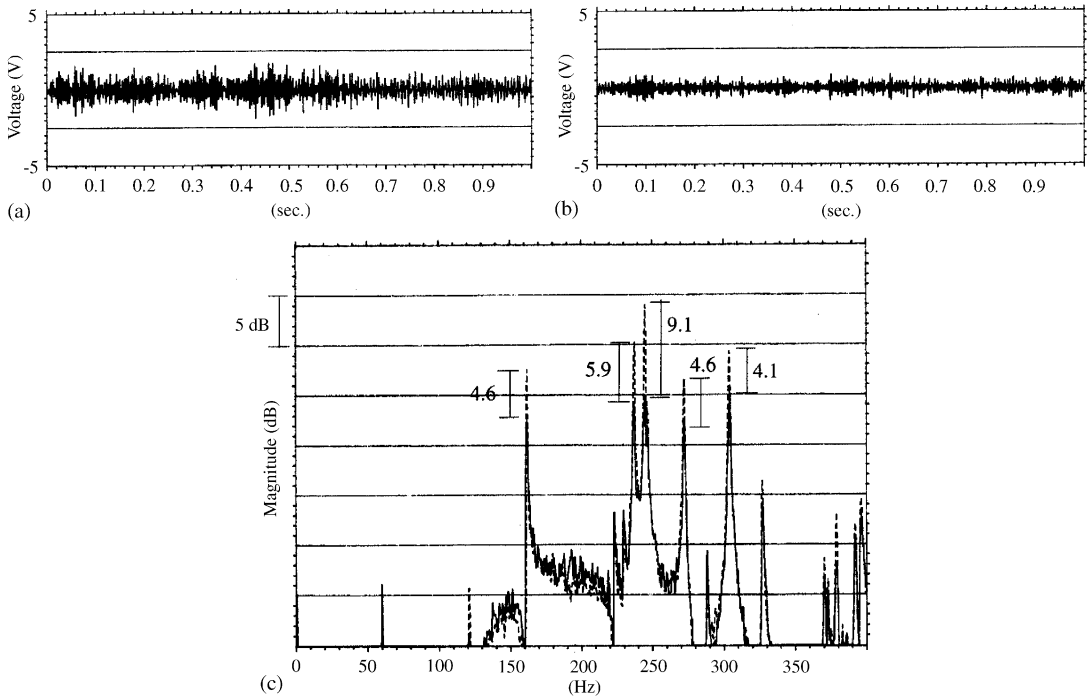

Fig. 9. Experimental result at sensor 1: (a) uncontrolled time response, (b) controlled time response, and (c) frequency response (uncontrolled and controlled).

10(c) show the frequency response comparing the uncontrolled signal with the controlled signal. From comparing Figs. 9(a) and 10(a) with Figs. 9(b) and 10(b), we can see the magnitudes of structural vibration of the control modes are attenuated by more than half. The attenuated results of structural vibration at each mode are summarized in Table 3. The control modes of S3, S4, and S5 are attenuated by amount of 9.1 dB maximum and 4.4 dB minimum.

The attenuated results of interior noise through the structural–acoustic coupling control are shown in Figs. 11 and 12. Fig. 11 shows the sound spectrum at the driver's hearing point, where the noise signal of 0–800 Hz is measured in the $\frac{1}{24}$ octave band. Because this position is near to the nodal plane of the first acoustic mode A1 (177 Hz), the noise peaks of S3 (162 Hz) and A1 cannot be shown well, but the noise near the structural mode S5 (272 Hz) can be measured very well due to effect of the acoustic mode A2 (257 Hz). The noise near to the structural mode S5 is attenuated by 5.8 dB, the overall noise is attenuated by 2.2 dB (from 70.3 to 68.1 dB), and the A-weighted noise is attenuated by 1.7 dBA. And Fig. 12 shows the sound spectrum at the rear seat's hearing point is near to the nodal plane of the second acoustic mode A2, where the noise of structural modes, S3, S5, and 304 Hz can be well measured. The noise of S3, S5, and 304 Hz is attenuated by 0.6, 3.4, and 3.6 dB, respectively, overall noise is attenuated by 1.7 dB (from 62.7 to 61.0 dB), and the A-weighted noise is attenuated by 1.1 dBA. Table 4 shows the experimental results of noise attenuation.

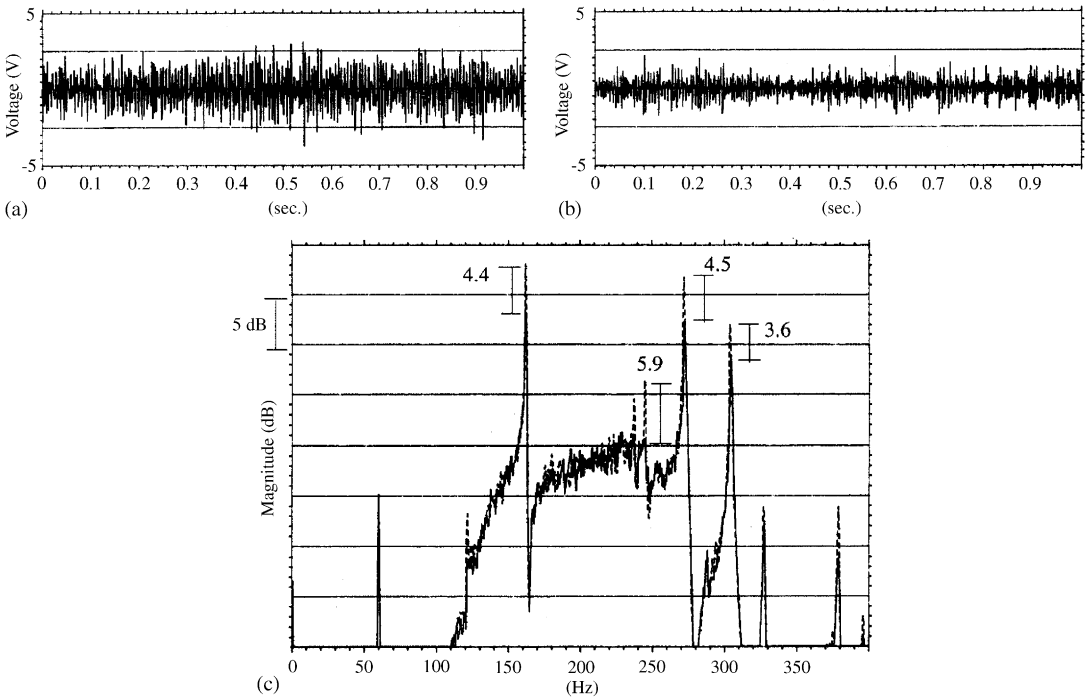

Fig. 10. Experimental result at sensor 2: (a) uncontrolled time response, (b) controlled time response, and (c) frequency response (uncontrolled and controlled).

Table 3
Experimental results at sensors 1 and 2

Mode	Natural freq. (Hz)	Vibration reduction (dB)	
		Sensor 1	Sensor 2
S3	162	4.6	4.4
—	236	5.9	3.4
S4	244	9.1	5.9
S5	272	4.6	4.5
—	304	4.1	3.6

5. Conclusion

The structural vibration control for a structural–acoustic coupling system was investigated using modal testing, the FEM, structural–acoustic modal coupling analysis, piezoelectric materials, and a robust LQG controller. By obtaining characteristics of interior noise with the coupling coefficients and modal parameters of the structural and acoustic system, the control plate and the control modes could be selected. A robust LQG controller with high- and low-pass filters was designed for effectively attenuating the interior noise of the cavity as well as the structural vibration of the cabin experimentally.

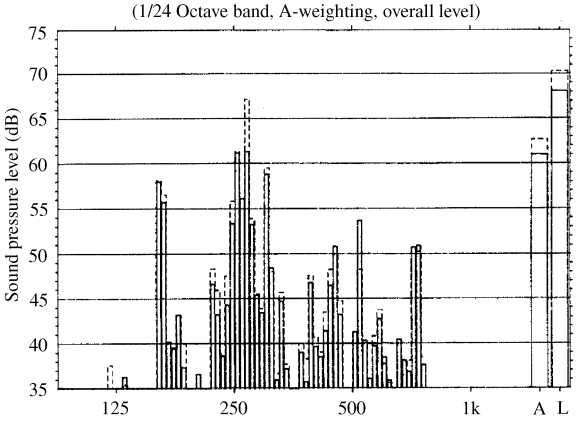

Fig. 11. Experimental result at microphone 1.

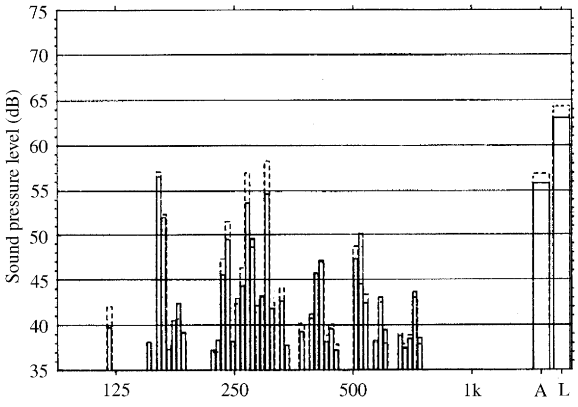

Fig. 12. Experimental result at microphone 2.

Table 4
Experimental result at microphones 1 and 2

Mode	Natural freq. (Hz)	SPL reduction (dB)	
		Microphone 1	Microphone 2
S3	162	0.1	0.6
—	236	0.2	1.7
S4	244	3.3	2.1
S5	272	5.8	3.4
—	304	0.7	3.6
A-weighted SPL		1.7 dBA	1.1 dBA
Overall SPL		2.2 dB	1.7 dB

Microphone 1: the driver's hearing point, microphone 2: the center hearing point of rear seat.

Acknowledgements

This work was supported by the Brain Korea 21 Project and the Korea Science/Engineering Foundation through the Research Center for Aircraft Pars Technology (ReCAPT), Gyeongsang National University, Korea.

References

[1] E.H. Dowell, Master plan for prediction of vehicle interior noise, American Institute of Aeronautics and Astronautics Journal 18 (4) (1980) 353–366.
[2] D.F. Nafske, et al., Structural–acoustic finite element analysis for the automotive passenger compartment: a review of current practice, Journal of Sound and Vibration 80 (2) (1982) 147–256.
[3] T.L. Richards, The Reduction of Structural Acoustic Coupling in Car Bodies, Ph.D. Thesis, Cranfield Institute of Technology, Cranfield, 1982.
[4] S.H. Kim, J.M. Lee, A practical method for noise reduction in a vehicle passenger compartment, American Society of Mechanical Engineers, Journal of Vibration and Acoustics 120 (1) (1998) 199–205.
[5] E.K. Dimitriadis, C.R. Fuller, Investigation of active control of sound transmission though elastic plate using piezoelectric actuators, AIAA 12th Aeroacoustic Conference, AIAA 89-1062, April 10–12, San Antonio, TX, 1989.
[6] C.R. Fuller, C.H. Hansen, S.D. Snyder, Experiments on active control of sound radiation from a panel using a piezoceramic actuator, Journal of Sound and Vibration 150 (2) (1991) 179–190.
[7] C.R. Fuller, C.A. Rogers, H.H. Robertshaw, Control of sound radiation with active/adaptive structures, Journal of Sound and Vibration 157 (1) (1992) 19–39.
[8] R.L. Clark, C.R. Fuller, Experiments on active control of structurally radiated sound using multiple piezoceramic actuators, Journal of the Acoustical Society of America 91 (6) (1992) 3313–3320.
[9] V.R. Sonti, J.D. Jones, Active vibration control of thin cylindrical shells using piezo-electric actuators, Proceedings of Recent Advances in Active Noise and Vibration Control, Blackshurg, VA, 1991, pp. 27–38.
[10] J.D. Jones, C.R. Fuller, Experiments on reduction of propeller induced interior noise by active control of cylinder vibration, Journal of Sound and Vibration 112 (2) (1987) 389–396.
[11] C.R. Fuller, C.H. Hansen, Active control of interior noise in model aircraft fuselages using piezoceramic actuators, AIAA 13th Aeroacoustics Conference, AIAA-90-3922, Tallahassee, FL, 1990.
[12] S.D. Snyder, C.H. Hansen, The design of systems to control actively periodic sound transmission into enclosed spaces, Part 1: analytical models, Journal of Sound and Vibration 170 (4) (1994) 433–449.
[13] S. Griffin, C. Hansen, B. Cazzolato, Feedback control of structurally radiated sound into enclosed spaces using structural error sensing, Journal of the Acoustical Society of America 106 (5) (1999) 2621–2628.
[14] D. Ewins, Modal Testing: Theory and Practice, Research Studies Press, Taunton, 1995.
[15] C.K. Song, J.M. Lee, J.K. Hwang, C.-H. Choi, Active vibration control of a thin plate using piezoelectric actuators/ sensors—multi-input multi-output control, 1997 SAE International Congress, SAE 970851, Detroit, MI, February 1997.
[16] J.K. Hwang, C.-H. Choi, C.K. Song, J.M. Lee, Robust LQG control of an all-clamped thin plate with piezoelectric actuators/sensors, IEEE/American Society of Mechanical Engineers Transactions on Mechatronics 2 (3) (1997) 205–212.
[17] J.K. Hwang, C.-H. Choi, C.K. Song, J.M. Lee, Identification of a thin plate with piezoelectric actuators and sensors, America Society of Mechanical Engineers, Journal of Vibration and Acoustics 120 (3) (1998) 826–828.
[18] CADA-X Rev 3.3, User manual LMS International, 1995, Leuven.
[19] Product Catalogs, Piezo Systems, Cambridge, MA, 1994.